Radical SAM enzyme QueE defines a new minimal core fold and metal-dependent mechanism

Citation: Dowling, Daniel P, Nathan A Bruender, Anthony P Young, Reid M McCarty, Vahe Bandarian, and Catherine L Drennan. "Radical SAM Enzyme QueE Defines a New Minimal Core Fold and Metal-Dependent Mechanism." Nat Chem Biol 10, no. 2 (December 22, 2013): 106–112.

As Published: http://dx.doi.org/10.1038/nchembio.1426

Publisher: Nature Publishing Group

Persistent URL: http://hdl.handle.net/1721.1/94563

Version: Author's final manuscript: final author's manuscript post peer review, without publisher's formatting or copy editing

Published in final edited form as:
Nat Chem Biol. 2014 February ; 10(2): 106–112. doi:10.1038/nchembio.1426.

Radical SAM enzyme QueE defines a new minimal core fold and metal-dependent mechanism

Daniel P. Dowling[1,2], **Nathan A. Bruender**[3], **Anthony P. Young**[3], **Reid M. McCarty**[3], **Vahe Bandarian**[3], and **Catherine L. Drennan**[1,2,4]

Catherine L. Drennan: cdrennan@mit.edu

[1]Howard Hughes Medical Institute, Massachusetts Institute of Technology, Cambridge, Massachusetts 02139

[2]Department of Chemistry, Massachusetts Institute of Technology, Cambridge, Massachusetts 02139

[3]Department of Chemistry and Biochemistry, The University of Arizona, Tucson, Arizona 85721

[4]Department of Biology Massachusetts Institute of Technology, Cambridge, Massachusetts 02139

Abstract

7-Carboxy-7-deazaguanine synthase (QueE) catalyzes a key *S*-adenosyl-L-methionine (AdoMet)- and Mg^{2+}-dependent radical-mediated ring contraction step, which is common to the biosynthetic pathways of all deazapurine-containing compounds. QueE is a member of the AdoMet radical superfamily, which employs the 5′-deoxyadenosyl radical from reductive cleavage of AdoMet to initiate chemistry. To provide a mechanistic rationale for this elaborate transformation, we present the first crystal structure of a QueE, along with structures of pre- and post-turnover states. We find that substrate binds perpendicular to the [4Fe-4S]-bound AdoMet, exposing its C6 hydrogen atom for abstraction and generating the binding site for Mg^{2+}, which directly coordinates to the substrate. The *Burkholderia multivorans* structure reported here varies from all other previously characterized members of the AdoMet radical superfamily in that it contains a hypermodified (β_6/α_3) protein core and an expanded cluster-binding motif $CX_{14}CX_2C$.

Keywords

Radical enzymes; X-ray crystallography; adenosylmethionine; tetrahydropterin; adenosylcobalamin; deazapurine

Correspondence to: Catherine L. Drennan, cdrennan@mit.edu.

Author Contributions

D.P.D. and C.L.D. designed and performed the crystallography experiments. N.A.B., R.M.M., A.P.Y., and V.B. designed and carried out the biochemical experiments. D.P.D, N.A.B., V.B., and C.L.D. contributed to the writing of the manuscript.

Competing Financial Interests

The authors declare no competing financial interests.

Accession codes

Protein coordinates and structure factors have been submitted to the Protein Data Bank under accession codes 4NJG, 4NJH, 4NJI, 4NJJ, and 4NJK.

Introduction

S-adenosyl-L-methionine (AdoMet or SAM) radical enzymes are a rapidly expanding superfamily: the estimated number was 600 in 2001[1], but more recent clustering methods[2] now place the number closer to 48,000. These [4Fe-4S]-containing proteins catalyze the reductive cleavage of AdoMet to generate the highly reactive and unstable oxidant 5′-deoxyadenosyl radical (dA•), which initiates a broad array of chemically complex reactions by H-atom abstraction from diverse substrates[3]. The radical AdoMet superfamily was originally identified on the basis of a conserved $CX_3CX\Phi C$ motif, in which Φ is an aromatic residue and Cys-thiolate side chains coordinate three of the Fe atoms of the essential [4Fe-4S] cluster[1]. Structures of all AdoMet radical enzymes solved to date show the adoption of either a full or a partial $(\beta/\alpha)_6$ triose-phosphate isomerase (TIM) barrel fold, which has been called an "AdoMet radical core"[4,5].

7-Carboxy-7-deazaguanine (CDG) synthase (QueE) catalyzes the unprecedented rearrangement of 6-carboxy-5,6,7,8-tetrahydropterin (CPH_4) into CDG with loss of ammonia, generating the pyrrolopyrimidine base of 7-deazapurines (Fig. 1). This reaction is the key step in transforming the purine base of GTP into the 7-deazapurine core structure that is found in >30 natural products and in the tRNA base queuosine (Fig. 1)[6,7]. QueE is an AdoMet radical enzyme, and like lysine 2,3-aminomutase and spore photoproduct lyase, AdoMet is used catalytically, i.e. reformed during each reaction cycle[8–10]. QueE from *B. subtilis* also has a clear dependence on Mg^{2+} ions[10], a newly reported feature for an AdoMet radical enzyme.

Here we report biochemical and X-ray crystal structure analyses of the QueE from *Burkholderia multivorans*. We find that this QueE has similar biochemical properties to the *B. subtilis* enzyme, but differs significantly in terms of structure: containing both a non-canonical cluster-binding motif ($CX_{14}CX\Phi C$) and a hypermodified protein fold. This work represents the first example of an AdoMet radical enzyme in which structural information is reported for all cofactors, the intact substrate, and product, making QueE from *B. multivorans* the best structurally characterized AdoMet radical enzyme to date as well as being one of the most divergent.

Results

B. multivorans QueE is a metal-dependent radical enzyme

Biochemically, the *B. multivorans* and *B. substilis* QueEs are quite similar. Both use AdoMet catalytically in the radical-based rearrangement of CPH_4 to CDG, and both show metal-dependence (Supplementary Results, Supplementary Fig. 1a,b). In terms of the former, assays of *B. multivorans* QueE reveal the production of greater than stoichiometric amounts of CDG compared to supplied AdoMet, supporting the catalytic use of AdoMet in this QueE as well (Supplementary Fig. 1a). In terms of the later, Mg^{2+} enhances activity of *B. multivorans* QueE by 3-fold, with a final k_{cat} value of 0.19 ± 0.06 min^{-1} (Supplementary Fig. 1b,c). Although the 3-fold activation observed is smaller than the ~10-fold activation found for the *Bacillus* protein, both QueEs display clear acceleration of activity in the presence of Mg^{2+}. Other cations, such as Na^+ or Mn^{2+} ions, show no acceleration of QueE activity (data not shown).

To initiate radical chemistry, all AdoMet radical enzymes require the one-electron reduction of the [4Fe-4S] cluster[11]. This electron is typically supplied by a flavodoxin[4,12–14]. For *B. multivorans* QueE, more product is generated using the chemical reductant dithionite than the commonly used *E. coli* flavodoxin/flavodoxin reductase system (Supplementary Fig.

1d); these results provide an unexpected difference with the *B. subtilis* enzyme[10], which displays the opposite trend.

B. multivorans QueE has a modified core fold

The crystal structure of QueE from *B. multivorans* complexed with AdoMet and 6-carboxypterin (6CP) was solved by single wavelength anomalous dispersion method to an R_{work} and R_{free} of 0.183 and 0.212, respectively (Supplementary Table 1). In the final 2.6 Å resolution structure, electron density is observed for all protein residues except for the N-terminal His_6-tag and the QueE starting methionine. Subsequent structures with ligands and metal ions were solved by isomorphous replacement using the initial protein model minus ligand atoms (Supplementary Table 2).

Both structurally and biochemically, QueE is a homodimer with each monomer displaying a variant of the $(\beta/\alpha)_6$ AdoMet radical fold (Fig. 2a,b and Supplementary Figs. 2,3). Of the structures determined to date, pyruvate formate-lyase activating enzyme (PFL-AE) is most similar to QueE overall, with an RMSD value determined by DALI of 2.7 Å for 171 Cα atoms[14,15] (Supplementary Table 3). Such structural conservation is unexpected between QueE and PFL-AE because their substrates are drastically different in size; QueE binds the small molecule CPH_4, while PFL-AE generates a glycyl radical within the protein pyruvate formate-lyase (PFL). However, the structures of PFL-AE from *E. coli* and QueE from *B. multivorans* are 246 and 210 residues in length, respectively, making them the smallest structural examples available of AdoMet radical enzymes, embodying the minimal core structure of this protein family.

In contrast to other AdoMet radical enzymes, including PFL-AE, the structural core of QueE, represented by a (β_6/α_3) architecture, is even more modest. Three α-helices (α3, α4, and α5) of the common AdoMet radical fold are replaced by short loops (L3 and L4) and by a short 3_{10}-helix (3_{10}H5) (Fig. 2a,b and Supplementary Fig. 2). These loops bury hydrophobic residues and are packed against the β-sheet, exposing backbone atoms and a few polar side chains to solvent (Supplementary Fig. 4). The replacement of these helices with loops has not been observed previously (see Discussion).

Structural features outside of the AdoMet radical core (Fig. 2a,b) are involved in substrate binding and oligomerization. QueE has a β-strand at the N-terminus of the protein (β1′) and both a 3_{10}-helix (3_{10}H1′) and a small β-strand (β2′) inserted between the cluster-binding loop and the first α-helix of the protein core (α1); at the C-terminus, it has a seventh β-strand and associated helix (β7′/α7′) (Fig. 2a and Supplementary Fig. 2). Interestingly, reciprocal interactions between the β1′–loop–β1 segment of QueE and the final β-strand (β7′) of the adjacent dimer molecule connect the beta sheet cores of the monomers, resulting in extension of the (β_6/α_3) protein core to an inter-monomer 10-stranded β-sheet resembling a crown (Fig. 2b,c). This expansion would presumably help stabilize this trimmed down core of the individual subunits. Although a similar β1′–loop–β1 segment is also observed in PFL-AE, PFL-AE is a monomer in solution and this protein segment interacts with its peptide substrate instead (Supplementary Fig. 5d)[14].

Another notable difference between some QueEs and other AdoMet radical enzymes occurs in the cluster-binding loop where a novel insert interrupts the canonical CxxxC sequence. 334 of 1589 QueE sequences contain an extended motif (Supplementary Fig. 6b). The vast majority of these insertions consist of fourteen residues ($CX_{14}CX\Phi C$), whereas two QueEs have twenty ($CX_{20}CX_2\Phi C$). Considering all 334 sequences, the consensus extended motif is $CNLW(S/T)GX_4(R/K)X_{2-8}(A/S)XCXFC$ (Supplementary Fig. 5a). The *B. multivorans* QueE structure reveals that this eleven-residue insertion adopts a 3_{10}-helical structure (3_{10}H1′) that extends away from the protein core (Fig. 2 and Supplementary Fig. 2).

Although it does not significantly alter the interactions between the Cys ligands and Fe atoms of the cluster, the insert leads to further burial and shielding of the [4Fe-4S] cluster from solvent (Supplementary Fig. 5b–e), as well as an increase in negative charge near the cluster (Supplementary Fig. 7).

AdoMet binding motifs conserved despite modified fold

The cluster-binding motifs of each monomer are located at opposite ends of the dimer molecule (Fig. 2a,c). Electron density for a complete [4Fe-4S] cluster within each monomer reveals that three of the Fe atoms from the cluster are coordinated by three cysteine residues from the $CX_{14}CX\Phi C$ motif. The remaining unique Fe binds the α-amino and α-carboxyl groups of AdoMet, which adopts an *anti* orientation about the glycosidic bond (Fig. 3 and Supplementary Figs. 8,9). Despite its modified fold, QueE employs all the structural motifs previously described for AdoMet binding: "GGE motif", the "ribose motif", the "β5 or GxIxGxxE motif", and the "β6 motif" (Fig. 3a and Supplementary Figs. 2,8)[4]. $G_{91}GE_{93}$ of the so-called "GGE motif" interact with the α-amino group of AdoMet and contain a *cis*-peptide linkage. The ribose moiety of AdoMet is within hydrogen bonding distance to the hydroxyl of S133, which is located within a "ribose motif" at the end of strand β4, and 3.4 Å from the amino group of K135. These residues are most likely involved in directing the formed dA• for correct H-atom abstraction, as the mutation of similar residues in biotin synthase leads to the formation of alternative products[16].

The adenine moiety of AdoMet is tightly packed against V151 of the "β5 motif" and F48 of the "cluster-binding loop motif" (Φ). The protein makes five hydrogen bonds with the adenine moiety of AdoMet from both the "β6 motif" (D176 and Q173) and the cluster-binding motif (F48 and D50) (Fig. 3a). Intriguingly, QueE is the first AdoMet radical structure in which a protein side chain (Q173) directly hydrogen bonds with the adenine moiety of AdoMet. An additional hydrogen bonding network is formed above the face of the adenine ring proximal to the substrate binding site between D50 of the cluster-binding loop, K149 of β5, D176 of β6, and Q202 and K205 of the β7′/α7′ C-terminal extension (Fig. 3a).

Structure with 6CP reveals location of active site

Structures of QueE complexed with AdoMet and 6CP reveal an intricate hydrogen-bonding network to position 6CP within the lateral opening of the partial barrel (Figs. 2a and 3b), consisting of residues located both within the N- and C-terminal extensions and the protein core. The pterin ring is further positioned in the active site by favorable π-π stacking interactions with noncore H204 and core F25. This binding mode positions an oxygen of the carboxylic acid moiety of 6CP close (3.2 Å) to the C5′ of AdoMet.

The C-terminus of the protein "plugs" the active site by making a unique hydrogen-bonding interaction between the carboxylic acid group of the C-terminal protein residue (P210) and both the N3 atom and exocyclic amine of the pterin ring (Fig. 3b). Despite having electron density for the entire protein chain except for M1, part of the active site remains slightly open to solvent near where radical generation would occur (Supplementary Fig. 10a), suggesting that binding of the reduced substrate, CPH_4, is accompanied by further small structural changes to fully close the active site and avoid side reactions.

Substrate binding generates a metal-binding site

In the 2.2 Å resolution crystal structure of QueE complexed with CPH_4, the substrate molecule is bound within the active site similarly to the binding mode observed with 6CP; however, the reduced ring system of the tetrahydropterin is not planar, directing the carboxylic acid moiety of CPH_4 away from the C5′ of AdoMet and towards R27 and T90 (Fig. 3c). This binding orientation positions C6 of the substrate closest to the C5′ of AdoMet

with a carbon-carbon distance of 3.9 Å, supporting the biochemical data that show dA• abstracts the H-atom at C6 to initiate catalysis[10]. Also, the side chain of Q13 rotates towards the substrate to form a hydrogen bonding interaction with the now protonated N8 of CPH_4.

With CPH_4 bound, the small active site opening that was observed in the 6CP-bound structure is now plugged with an apparent mononuclear ion (Fig. 3c, Supplementary Fig. 10b). Given the observed Mg^{2+} dependence of QueE chemistry, we considered whether this putative metal-binding site could be the location to which catalytic Mg^{2+} binds. Anomalous dispersion is an excellent tool for confirming that metal ions are bound at putative metal-binding sites in crystal structures. Unfortunately, neither the Na^+ ions that were present in the crystallization buffer nor the physiologically relevant Mg^{2+} ions have a strong anomalous signal. Thus, to confirm assignment of this putative metal-binding site, Mn^{2+}-QueE was used. Anomalous data collected at a wavelength of 1.7399 Å for crystals of QueE soaked with 0.1 M $MnSO_4$ revealed anomalous signal for two Mn^{2+} ions per QueE molecule. The first Mn^{2+} is bound in the same site described above, confirming that this is a metal-binding site (Fig. 4a); the second is bound on the surface of the protein (Supplementary Fig. 11).

With Mn^{2+} anomalous data corroborating the relevance of this site for metal binding, QueE crystals grown in the presence of 50 mM $MgCl_2$ allowed for the first description of a catalytic metal ion site in an AdoMet radical enzyme. The ligand environment about Mg^{2+} is pseudo-octahedral, with three water ligands (H_2O-A,-B, and -C), the substrate C4 carbonyl and C6 carboxylate oxygens, and the hydroxyl of T51 (Fig. 4b). This threonine, which follows the cluster-binding loop, may be activated for metal coordination by the carboxylate of D50 (Fig. 3c, 4b). Although T51 is the only residue to interact directly with the metal ion, H_2O-A and -B ligands to Mg^{2+} are involved in hydrogen bonding interactions with nearby residues (E15, D50 and H204). Metal ion-ligand distances are slightly longer than expected for a tightly coordinated Mg^{2+} ion (Supplementary Table 4)[17,18], potentially due to the partial occupancy of this site by Na^+ ions, which were also present in the crystallization solution.

In terms of metal ion specificity, neither Mn^{2+} or Na^+ increase QueE activity (data not shown) and neither show identical binding interactions as Mg^{2+}. While hard-soft acid-base theory predicts that Mg^{2+} favors hard ligands such as oxygen, Mn^{2+} readily interacts with both oxygen and nitrogen. Presumably because of this property, Mn^{2+} directly coordinates the cyclic N5 of the substrate with a distance of 2.0 Å (Fig. 4a). Although Mn^{2+} also interacts with the substrate carbonyl and carboxylate moieties, and H_2O-B and –C, the distance to T51 is long (~3.6 Å), and water A is not observed (Supplementary Table 4)[17,18].

The structure of QueE solved with Mg^{2+} also shows subtle differences relative to the structure solved with Na^+ (Fig. 4b,c and Supplementary Table 4). In particular, only Mg^{2+} appears to interact favorably with both the substrate carboxylate (~3.0 Å) and carbonyl moieties (2.9 Å), whereas the distance is longer between Na^+ and the substrate carbonyl (3.4 Å). Interestingly, the C4a-N5-C6-C torsion angle of substrate varies by ~30° for Mg^{2+} and Mn^{2+} compared to Na^+ (Fig. 4d).

Hydrogen-bonding network maintained in CDG-bound QueE

The structure of QueE co-crystallized with AdoMet and product, CDG, provides a comparison between how substrate and product bind (Figs. 3c,d and 4b,e,f). There are little to no changes in the structure, including the protein residues in the active site, with an RMSD for 208 Cα atoms of the protein dimer of 0.120 Å. CDG and CPH_4 are bound similarly; however, the smaller size and strictly planar nature of CDG leads to slightly altered ring rotation (~30°) and somewhat altered interactions (Fig. 4f). In particular, the

Mg^{2+} is coordinated by the C7-carboxylate of CDG in a monodentate fashion (2.2 Å), while maintaining similar interactions with the carbonyl moiety of CDG, the hydroxyl of T51, and three water molecules as in the CPH_4-bound structure (Fig. 4e). Conversion of CPH_4 to CDG most likely proceeds through a *gem*-amino carboxylic acid pyrrole-like intermediate, and modeling of this intermediate places the proposed exocyclic C7 nitrogen radical proximal to the C5′ of AdoMet, poised to abstract an H-atom from bound dA-H, which would regenerate the AdoMet cofactor (Fig. 4g).

Discussion

The structure of the *B. multivorans* QueE reveals a new protein architecture for an AdoMet radical enzyme that represents a drastic deviation from the $(\beta/\alpha)_6$ "AdoMet radical core" fold[4]. Here we find that QueE performs AdoMet radical chemistry with a "pared-down" β_6/α_3 architecture and a unique insertion into the canonical $CX_3CX\Phi C$ cluster binding motif. The *B. multivorans* QueE structure is not the first report of a modified TIM barrel, as the majority of AdoMet radical enzymes are TIM-fold variants, but to the best of our knowledge this type of alteration is unprecedented in this or any enzyme superfamily. Previously, a structure of a "Tiny TIM" from the hyperthermophile *Pyrococcus woesei* was reported, which yielded a glimpse of a trimmed down TIM barrel consisting of only 228 amino acids in comparison to the average of 298 residues[19,20]. Tiny TIM has shorter α-helices and loops, but still retains all eight α-helices. Structures also have been reported with "distorted TIM barrel" folds[21–27]. In all cases where modifications to the barrel core have been reported, the variations involve either the full deletion of a (β/α) unit or the replacement of an α-helix by additional protein material; therefore, the deletion of three α-helices in QueE from *B. multivorans* is even more surprising.

Part of the reason that these deletions are unanticipated is that an analysis of TIM barrel structures predicts that α-helices are required to provide conformational flexibility to the rigid barrel frame[28]. In contrast to helices, the short L3 and L4 loops of QueE would not be predicted to contain a great deal of flexibility due to their limited length in connecting β-strands of the partial barrel, and thus this substitution of helices by loops is unexpected. However, the B-factor values (a measure of thermal disorder in $Å^2$) of these loops are not that different from the α-helices, indicating that the loops may just be long enough (Supplementary Fig. 4a). Thus, with the correct design of the loop, the substitution may allow for the requisite flexibility.

The structure of QueE from *B. multivorans* is also the first example of an AdoMet radical enzyme displaying a substantially modified cluster-binding motif. We find that the eleven-residue insertion adopts a 3_{10}-helix that is oriented above the barrel and [4Fe-4S] cluster. Although other sequences for binding the cluster have been reported[29–31], they contain only minor modifications, e.g. $CX_5CX\Phi C$ in HmdB[30] compared to the standard $CX_3CX\Phi C$. Other reported differences include the presence of a slightly modified CX_2CX_4C motif in ThiC on a separate domain rather than on a loop that follows β-strand 1 of the AdoMet radical core[29]. Importantly, the modified $CX_{14}CX\Phi C$ motif in *B. multivorans* QueE is not essential for the CDG synthase reaction given that other QueEs (e.g. *Bacillus subtilis* in Supplementary Figs. 2 and 6) contain the traditional $CX_3CX\Phi C$ motif. Instead, we propose that this eleven-residue insert, along with loops L3 and L4, controls specificity of the *B. multivorans* QueE for its protein reductase. Flavodoxin is a common reductase for AdoMet radical enzymes and is believed to bind near the cluster-binding motif and helices 3 and 4 of the "core" fold[4,12–14], i.e., the regions that are modified in this QueE (Supplementary Fig. 7). Nonetheless, we expect that flavodoxin will bind to the *B. multivorans* enzyme in this same general location, since despite the protein modifications, this site still represents the closest binding surface to the [4Fe-4S] cluster for electron transfer. However, differences in

the shape complementarity and electrostatics in the QueE from *B. multivorans* may impair the ability of certain flavodoxins to bind and reduce this enzyme. Consistent with this notion, more CDG is detected when *B. multivorans* is incubated with dithionite than with *E. coli* flavodoxin/flavodoxin reductase system (Supplementary Fig. 1d). Further studies with flavodoxins from *B. multivorans* and other species will aid in determining whether modification of the cluster-binding loop and of barrel helices accompanies the evolution of protein-protein interaction of AdoMet radical enzymes with their respective physiological reductant.

The conversion of CPH_4 to CDG by QueE is extremely challenging chemistry. The enzyme must activate a tetrahydropterin to convert its tetrahydropyrazine ring into a five-membered pyrrole ring with loss of ammonia. Stable isotope experiments have previously shown that the reaction entails abstraction of the C6 hydrogen of the substrate by dA•, and that in the course of conversion of CPH_4 to CDG, the *pro-R* C7 hydrogen is lost to solvent[10]. The Mg^{2+} dependence of the reaction, which was first noted with the *Bacillus* protein[10] but is also observed here with the *Burkholderia* homolog, was enigmatic. These structures of the *Burkholderia* protein with 6CP substrate analog, CPH_4, and CDG, solved in the presence of Mg^{2+}, provide exquisite molecular level detail of the active site, confirming and extending the biochemical findings.

A mechanistic proposal that incorporates structural findings is shown in Fig. 5. The X-ray crystal structure confirms that the C5′ of the dA moiety of AdoMet is close (3.8 Å) to the substrate C6, poised to abstract the C6 hydrogen upon reductive cleavage of AdoMet in steps **I→II**. Mg^{2+} may facilitate this H-atom abstraction through its interaction with both the carbonyl and carboxylate moieties of the substrate. Following substrate radical formation, a number of routes are possible to generate the 5-membered pyrrole ring, all of which are reminiscent of group migration reactions catalyzed by adenosylcobalamin-dependent and AdoMet radical mutases[32]. By analogy to lysine aminomutases[9], one may envision a migration *via* an azocyclopropyl radical intermediate **III-A** that is stabilized by resonance. Alternatively, the rearrangement may proceed by ring opening in **III-B** followed by a 5-*exo trig* ring-closure, resulting in the pyrroline ring. Next, the amino-centered radical **IV** would reabstract a hydrogen atom from dA-H to reform AdoMet for use in a subsequent catalytic cycle, forming a *gem*-amino carboxylate pyrrole-like ring **V** that is modeled in Figure 4g. The following step, elimination of the amino group in **V→VII**, must be enzyme catalyzed based on the stereoselective loss of deuterium from the substrate C7 position[10]. Here, enzyme-bound Mg^{2+} could act as a Lewis acid facilitating path **VI→VII-A**; alternatively, the protein C-terminal carboxylic acid group (P210) could promote path **V→VII-B** through its interaction with the six-membered ring of substrate. Subsequent deprotonation of the *Pro-R* C8 proton of either **VII-A** or **VII-B** would lead to the final aromatized product **VIII**. E116 is positioned nearby (Fig. 4f,g) and is likely responsible for this deprotonation.

Mg^{2+} is not a “spectator” in this reaction and is likely to play a role at more than one step in this complex chemical transformation. These structures suggest that Na^{+} and Mn^{2+} cannot substitute for Mg^{2+} due to their differential interactions with substrate, either the loss of coordination with the carbonyl moiety of substrate or the gain of interaction with a ring nitrogen, respectively. Divalent and monovalent metals are known to assist in adenosylcobalamindependent chemistry[33–35], but the QueE reaction is the first characterized example for the AdoMet radical superfamily. Importantly, no sequence motif exists for the Mg^{2+} binding site with only one protein residue involved in coordination. Thus, identification of metal-dependent activities of other AdoMet radical enzymes must await biochemical characterization.

Once called a "poor man's adenosylcobalamin" due to the relatively inexpensive nature of its biosynthesis[36], AdoMet bound to a [4Fe-4S] cluster has proven to be a ubiquitous catalyst for spectacular chemical transformations. With only 210 amino acids, *B. multivorans* QueE represents a kind of "poor man's AdoMet radical enzyme," whose structure has caused us to reconsider key features of AdoMet radical enzyme structure and reactivity. This QueE structure challenges the idea that the size of an AdoMet radical enzyme is inversely correlated to its substrate's size[14]. Here we find that QueE is most similar to PFL-AE in terms of structure but the two are not at all equivalent in terms of the sizes of their substrates. More importantly, this QueE structure prompts us to question the use of the $CX_3CX\Phi C$ sequence motif as the defining feature of an AdoMet radical enzyme. The *B. multivorans* QueE structure indicates that $CX_3CX\Phi C$ cysteine spacing is not required for the canonical binding of AdoMet or for AdoMet radical chemistry. Although impossible to predict by sequence alignments, the QueE structure also reveals that an AdoMet radical core fold can be established without three of the six α-helices. Recent work on another AdoMet radical enzyme, BtrN, further shows that the sixth strand of the $(\beta/\alpha)_6$ barrel can also be deleted without significantly altering AdoMet binding[37]. Thus, bioinformatic analyses of AdoMet radical enzymes must consider protein sequences with expanded cluster-binding motifs and contracted core folds. Currently, the predicted 48,000 unique AdoMet radical enzyme sequences map to a vast area of sequence space (Supplementary Fig. 6), presumed to reflect a great array of chemical reactivities and substrate specificities. Although much of this sequence variation is undoubtedly due to the above, this work reminds us that two enzymes with identical functions are not necessarily close in sequence space. This work also suggests that AdoMet radical enzymes may have evolved to recognize different protein reductases, and that some of the magnitude of sequence diversity may be due to the latter. Finally, this series of structures provides long-awaited snapshots of an AdoMet radical reaction, providing a template for mechanistic considerations and computational investigations of this stunning radical-based chemistry.

Online Methods Section

Protein overexpression and purification

The *E. coli* codon-optimized gene encoding *B. multivorans* QueE was obtained from GenScript (Piscataway, NJ) (Supplementary Fig. 12). The gene was excised from the supplied pUC57 with *NdeI* and *HindIII* and ligated into a similarly digested pET28a vector for expression of the N-terminal His_6-tagged protein. *E. coli* BL21(DE3) cells were co-transformed with the QueE expression vector and pDB1282[38] for enhanced [4Fe-4S] cluster biosynthesis. Cells were grown in LB containing 34 μg/mL kanamycin and 100 μg/mL ampicillin at 37 °C. At OD_{600} ~0.3, arabinose and iron(III) chloride were added to a final concentration of 0.05 % (w/v) and 50 μM, respectively. At OD_{600} ~ 0.5 expression of QueE was induced by the addition of isopropyl β-D-1-thiogalactopyranoside to a final concentration of 0.1 mM. Cells were harvested 6 h after induction and flash frozen.

Recombinant QueE was purified and reconstituted in an anaerobic chamber (Coy Lab Products) under 5% H_2/95% N_2. Cells were resuspended in buffer containing 50 mM potassium phosphate (pH 7.4), 0.5 M potassium chloride, 50 mM imidazole, and 1 mM phenylmethylsulfonyl fluoride (buffer A) and lysed via a digital sonifier (Branson) operated at 50% amplitude. The resulting lysate was centrifuged at 18,000 × *g* for 30 min at 4 °C to clear the cellular debris from the lysate. His_6-tagged protein was purified from the soluble lysate with a 1 mL HisTrap™ HP column (GE Healthcare) charged with nickel sulfate. The column was equilibrated with buffer A prior to loading the supernatant, washed with 5 column volumes of buffer A, and eluted with a linear gradient from 0 to 100% buffer B (buffer A supplemented with 0.5 M imidazole) in a total of 10 mL. Fractions containing

QueE were pooled, concentrated to 3 mL, and desalted into 50 mM PIPES (pH 7.4) and 10 mM DTT using an Econo-Pac 10DG column (Bio-Rad). The purified enzyme was then reconstituted by rapidly adding 8 molar equivalents of iron(III) chloride and sodium sulfide and incubated at room temperature for 4 h. The reconstitution reaction was centrifuged to remove precipitate and the reconstituted protein was desalted in the same manner as previously described. Protein concentration was determined by Bradford method with BSA as the standard. The final reconstituted and desalted enzyme was >95% pure by SDS PAGE analysis. Protein was flash frozen in aliquots and stored at −80 °C.

Size-exclusion Chromatography

To determine the oligomerization state of *B. multivorans* QueE, reconstituted protein was injected (0.5 mL of 6 mg/mL protein) onto a HiPrep 16/60 Sephacryl S-200 high-resolution size exclusion column (GE Healthcare) equilibrated in 50 mM PIPES (pH 7.4) and 10 mM DTT. The column was operated at 1 mL/min at room temperature in an anaerobic chamber (Coy Lab Products) under 5% H_2/95% N_2. QueE was injected onto the column two times, once alone and once with size exclusion standards (Bio-Rad) that included bovine thyroglobulin (670 kDa), bovine γ–globulin (158 kDa), chicken ovalbumin (44 kDa), horse myoglobin (17 kDa), and vitamin B_{12} (1.35 kDa). The standards were also injected onto the column alone. The elution volume of QueE was compared to the elution volumes of the standard to obtain the approximate molecular weight of the protein.

QueE activity assays

The purified N-terminally His_6-tagged enzyme was assayed for activity as follows. Assays contained 50 mM PIPES (pH 7.4), 10 mM DTT, 10 mM dithionite, 2 mM AdoMet (enzymatically synthesized and purified as previously described[10]; >95% pure by HPLC at 259 nm), 2 mM $MgSO_4$, QueE and 2 mM CPH_4 (enzymatically synthesized and purified as previously described[10]; >99% pure by HPLC at 298 nm). Aliquots (60 μL) were withdrawn, quenched with 6 μL of 30% (w/v) TCA and analyzed by HPLC. An aliquot (60 μL) was injected onto an Agilent Zorbax Eclipse C-18 column (4.6 mm × 250 mm) pre-equilibrated in 0.1 % (v/v) TFA. Analyte components were eluted over 40 min with a linear gradient from 0 to 6% acetonitrile with 0.1 % (v/v) TFA at a flow rate of 0.75 mL/min, monitoring the elution profile from 200 to 500 nm using a photodiode array detector. The peak area corresponding to CDG was converted to concentration of CDG via a calibration curve constructed by injecting known amounts of CDG onto the C-18 column. All reactions were run in triplicate and the data are represented by the mean values; errors are the standard deviation of the triplicate data. In all of the reactions, all components except CPH_4 were mixed and incubated at room temperature for 10 min. Reactions were initiated upon addition of CPH_4. To determine the optimal reductant, assays with 5 μM QueE were conducted in the presence of either 10 mM dithionite or 40 μM flavodoxin/flavodoxin reductase with 2 mM NADPH to compare the amount of CDG formed after 30 min, run in triplicate. To determine the k_{cat}, the [QueE] was varied at 2, 4, 7, and 10 μM under saturating AdoMet, CPH_4 and Mg^{2+} conditions. For the Mg^{2+} activation assays, reactions were set up with 2 μM QueE and 0 or 2 mM $MgSO_4$. In these assays, AdoMet (Sigma-Aldrich; >75% pure) was used because of a magnesium contamination in the enzymatically synthesized AdoMet.

Stoichiometric requirement of AdoMet

To determine the stoichiometric requirement of AdoMet, a reaction was prepared as described above, except that 10 μM enzymatically prepared AdoMet and 10 μM QueE were used in a total reaction volume of 0.22 mL. The reaction was initiated by addition of substrate after incubating QueE in the presence of dithionite and AdoMet for 10 min.

Aliquots (40 μL) were withdrawn at 5, 60, 180, 360, and 540 min, quenched with 4 μL of 30% (w/v) TCA, and analyzed by HPLC, as described above.

Crystallization

Crystallization conditions were identified at 21 °C using a Mosquito pipetting robot (TTP LabTech) housed within an anaerobic chamber (MBraun) under a nitrogen atmosphere (O_2 < 0.1 ppm) and optimized in an anaerobic chamber (MBraun) at either 21 °C or 4 °C. All solutions larger than 100 μL were purged with argon for greater than 30 min. Volumes smaller than 100 μL were frozen, exposed to vacuum, brought into the anaerobic chamber and allowed to thaw and gas exchange before use. AdoMet was enzymatically synthesized and purified as previously described[10] (>99% pure by HPLC at 298 nm), and 6-carboxypterin (6CP; Sigma Aldrich; >98 % purity) was used without further purification. 6-carboxy-5,6,7,8-tetrahydropterin (CPH_4; >99% purity by HPLC at 298 nm) and 7-carboxy-7-deazaguanine (CDG; > 95% purity by HPLC at 300 nm) were generated and purified as previously described[10].

Initial crystals of QueE in complex with 6CP and AdoMet formed at 21 °C by mixing 0.1 μL protein solution [13.9 mg/mL QueE in 50 mM PIPES (pH 7.4) and 10 mM DTT, 5 mM AdoMet, and 5 mM 6CP; added in that order] and 0.1 μL of precipitant solution [2.0 M NaK_2PO_4 (pH 6.8) and 0.1 M sodium acetate (pH 4.5)] over a 70 μL reservoir. Protein solutions were centrifuged prior to setting up crystal trays to remove insoluble 6CP. Crystals of 50 μm × 100 μm × 30 μm dimensions formed within a week. Crystals were optimized using sitting drop vapor diffusion method, and crystals formed in both 1:1 and 3:1 ratios of protein to precipitant solution with a final drop size of 2 μL. Crystals were transferred to an anaerobic chamber (Coy Lab Products) under 95% argon, 5% hydrogen at 24 °C, harvested and cryoprotected in 2.6 M NaK_2PO_4 (pH 6.8), 50 mM sodium acetate (pH 4.5), and 10 % glycerol. All crystals were then cryocooled in liquid nitrogen within an anaerobic chamber (Coy Lab Products).

QueE complexed with AdoMet and CPH_4, with or without Mg^{2+} [13.9 mg/mL QueE in 50 mM PIPES (pH 7.4) and 10 mM DTT, 5 mM AdoMet and 5 mM CPH_4, ± 50 mM $MgCl_2$; added in that order] formed optimal crystals between 1.8 – 2.2 M NaK_2PO_4 (pH 6.8) and 0.1 M sodium acetate (pH 4.5) at 4 °C. Crystals without $MgCl_2$ present have a similar morphology to those grown with 50 mM $MgCl_2$. QueE complexed with CDG and Mg^{2+} were obtained using identical conditions. All crystals were cryoprotected and flash cooled anaerobically with 2.6 M NaK_2PO_4 (pH 6.8), 50 mM sodium acetate (pH 4.5) and 10 % glycerol, ± 25 mM $MgCl_2$.

Crystal soaking experiments with Mn^{2+}

Crystals grown in a 4 °C MBraun anaerobic chamber in the presence of AdoMet and CPH_4, but in the absence of $MgCl_2$ (see above), were used for Mn^{2+} soaking experiments. In order to obtain a structure of QueE with Mn^{2+} ions, it was necessary to exchange the crystallization condition [2.0 M NaK_2PO_4 (pH 6.8) and 0.1 M acetate (pH 4.6)] before addition of excess Mn^{2+} ions to prevent formation of salt precipitates within the drop. Buffer exchange was achieved by streaking crystals of QueE through a 10 μL drop of stabilization buffer [0.1 M HEPES and 30% v/v Jeffamine ED-2001 (pH 7.0)] prior to transferring crystals into the same solution supplemented with 0.1 M $MnSO_4$. After 12 hrs, crystals were backsoaked briefly in stabilization solution and directly cryocooled in liquid nitrogen.

X-ray diffraction data, structure determination and refinement

Diffraction data for QueE with AdoMet and 6CP were collected on a RAxis IV++ detector with Rigaku MicroMax007-HF rotating anode, and a higher resolution data set was collected

at the National Synchrotron Light Source (NSLS, Brookhaven, X25). Data were collected, indexed, integrated, and scaled in space group $P4_32_12$, with 2 molecules in the asymmetric unit, using the software HKL2000[39] (Supplementary Table 1). Phases were determined by single-wavelength anomalous dispersion methods with data collected at the Cu Kα edge (1.54178 Å) for QueE complexed with AdoMet and 6CP. The data displayed good anomalous signal to approximately 5 Å resolution, and the program SOLVE in phenix AutoSol[40] identified two sites with occupancies greater than 1.0, indicative of two [4Fe-4S] clusters per dimer in the asymmetric unit. Sites were refined and experimental electron density maps were generated using the program SHARP/autoSHARP[41], with an overall figure-of-merit of 0.47 to 5.0 Å resolution. The resulting figure-of-merit weighted electron density map yielded interpretable electron density for building protein secondary structure.

Secondary structure elements were built into electron density maps in the program COOT[42], using the structure of AdoMet radical enzyme pyruvate formate-lyase activating enzyme (PFL-AE, PDB accession code 3CBA)[14] as a guide. The resulting QueE model was used to update the mask generated in SHARP for solvent flattening and phase extension in steps of ~0.5 Å to 3.1 Å resolution, allowing for completion of a poly-alanine model. The addition of side chains was carried out using the cluster-binding motif and [4Fe-4S] cluster as initial anchors for the protein sequence. Initial refinement protocols at 3.1 Å resolution consisted of rigid body refinement, followed by deformable elastic network assisted simulated annealing refinement in CNS version 1.3[43], applying non-crystallographic symmetry (NCS) restraints for all atoms. Following iterative rounds of refinement (using simulated annealing, energy minimization and B-factor refinement protocols in phenix and/or CNS 1.3 without sigma cutoff[44–46]) and model building in COOT[42], phases were extended to the full 2.9 Å resolution of the "R-axis" data. The subsequent QueE model was refined similarly against an isomorphous "NSLS" 2.6 Å resolution remote dataset, following truncation of this data using the French and Wilson method in the ccp4 suite of programs[47,48]. Toward the end of the refinement process, NCS restraints were released from all atoms, alternate side chain conformations were identified, and TLS restraints were used (seven per molecule, determined by the TLS Motion Determination Server[49,50]). Water and ligand molecules were added in later rounds of refinement, and composite omit maps were generated to verify the structure. The final protein model contained all residues except for the N-terminal His_6-tag and initial methionine (residues T2-P210), and analysis of the Ramachandran plot by Procheck indicates 87.9% of non-glycine and non-proline residues are in the most favored regions, and no residues are in the generously allowed or disallowed regions[51].

The resulting structure of AdoMet/6CP QueE, minus metal, water and ligand atoms, was used to solve structures of AdoMet/CPH_4-Na^+ (Advanced Photon Source, APS; 24ID-C; Pilatus 6MF), AdoMet/CPH_4-Mg^{2+} (APS; 24ID-E; ADSC Q315), AdoMet/CPH_4-Mn^{2+} (APS; 24ID-C; Pilatus 6MF), and AdoMet/CDG-Mg^{2+} (APS; 24ID-C; Pilatus 6MF) by isomorphous replacement. Structures were built and refined using identical protocols as described above with the same R_{free} test sets (5%, originating from the AdoMet/6CP-bound dataset). Refinement statistics are presented in Supplementary Table 2. All structures contain residues T2-P210, with only the N-terminal affinity tag and initial methionine missing from the model.

Small molecule topology and definition files for 6CP, CPH_4, CDG, and AdoMet were generated using the Grade Web Server (http://grade.globalphasing.org). Protein figures were generated using PyMOL, and electrostatic calculations were performed with the APBS[52] plugin within PyMOL. Topology diagrams were generated using the software TOP in the CCP4 suite of programs[53], and graphs were generated in the software PRISM. Sequence similarity diagrams were generated using the software Cytoscape[54] with protein sequences obtained from the Structure Function Linkage Database[2].

Supplementary Material

Refer to Web version on PubMed Central for supplementary material.

Acknowledgments

This work was supported by NIH GM72623 (V.B.) with Administrative Supplement GM72623 S01 to V.B. for the collaboration between V.B. and C.L.D; a Career Award in Biomedical Sciences from the Burroughs Wellcome Fund (V.B.); a Biological Chemistry Training Grant (GM008804) (R.M.M.); and C.L.D is a Howard Hughes Medical Investigator. This work is based upon research conducted at beamline X25C of the National Synchrotron Light Source (NSLS) and at the Advanced Photon Source (APS) on the Northeastern Collaborative Access Team (NE-CAT) beamlines. Financial support from NSLS comes from the Offices of Biological and Environmental Research and of Basic Energy Sciences of the US Department of Energy, and from the National Center for Research Resources (P41RR012408) and from the National Institute of General Medical Sciences at the National Institutes of Health (P41GM103473). NE-CAT at APS is supported by grants from the National Center for Research Resources (5P41RR015301-10) and the National Institute of General Medical Sciences at the National Institutes of Health (8 P41 GM103403-10). APS is an Office of Science User Facility operated for the U.S. Department of Energy (DOE) Office of Science by Argonne National Laboratory, and is also supported by the U.S. DOE under Contract No. DE-AC02-06CH11357. We thank Dr. Gemma L. Holliday and Professor Patsy Babbitt (UCSF) and the Enzyme Function Initiative for their analysis of sequences in the AdoMet radical enzyme superfamily, which are available from the Structure Function Linkage Database (http://sfld.rbvi.ucsf.edu/django/superfamily/29/).

References

1. Sofia HJ, Chen G, Hetzler BG, Reyes-Spindola JF, Miller NE. Radical SAM, a novel protein superfamily linking unresolved steps in familiar biosynthetic pathways with radical mechanisms: functional characterization using new analysis and information visualization methods. Nucleic Acids Res. 2001; 29:1097–1106. [PubMed: 11222759]
2. Pegg SC-H, et al. Leveraging enzyme structure-function relationships for functional inference and experimental design: the structure-function linkage database. Biochemistry. 2006; 45:2545–2555. [PubMed: 16489747]
3. Shisler KA, Broderick JB. Emerging themes in radical SAM chemistry. Curr.Opin.Struct.Biol. 2012; 22:701–710. [PubMed: 23141873]
4. Vey JL, Drennan CL. Structural insights into radical generation by the radical SAM superfamily. Chem. Rev. 2011; 111:2487–2506. [PubMed: 21370834]
5. Dowling DP, Vey JL, Croft AK, Drennan CL. Structural diversity in the AdoMet radical enzyme superfamily. BBA - Proteins and Proteom. 2012; 1824:1178–1195.
6. McCarty RM, Somogyi Á, Lin G, Jacobsen NE, Bandarian V. The deazapurine biosynthetic pathway revealed: In vitro enzymatic synthesis of PreQ0 from guanosine 5'-triphosphate in four steps. Biochemistry. 2009; 48:3847–3852. [PubMed: 19354300]
7. McCarty RM, Bandarian V. Biosynthesis of pyrrolopyrimidines. Bioorg.Chem. 2012; 43:15–25. [PubMed: 22382038]
8. Cheek J, Broderick JB. Direct H atom abstraction from spore photoproduct C-6 initiates DNA repair in the reaction catalyzed by spore photoproduct lyase: Evidence for a reversibly generated adenosyl radical intermediate. J. Am. Chem. Soc. 2002; 124:2860–2861. [PubMed: 11902862]
9. Frey PA, Reed GH. Pyridoxal-5′-phosphate as the catalyst for radical isomerization in reactions of PLP-dependent aminomutases. BBA - Proteins and Proteom. 2011; 1814:1548–1557.
10. McCarty RM, Krebs C, Bandarian V. Spectroscopic, steady-state kinetic, and mechanistic characterization of the radical SAM enzyme QueE, which catalyzes a complex cyclization reaction in the biosynthesis of 7-deazapurines. Biochemistry. 2013; 52:188–198. [PubMed: 23194065]
11. Duschene KS, Veneziano SE, Silver SC, Broderick JB. Control of radical chemistry in the AdoMet radical enzymes. Curr.Opin.Chem. Biol. 2009; 13:74–83. [PubMed: 19269883]
12. Layer G, Moser J, Heinz DW, Jahn D, Schubert W?D. Crystal structure of coproporphyrinogen III oxidase reveals cofactor geometry of Radical SAM enzymes. EMBO J. 2003; 22:6214–6224. [PubMed: 14633981]

13. Berkovitch F, Nicolet Y, Wan JT, Jarrett JT, Drennan CL. Crystal structure of biotin synthase, an *S*-adenosylmethionine-dependent radical enzyme. Science. 2004; 303:76–79. [PubMed: 14704425]
14. Vey JL, et al. Structural basis for glycyl radical formation by pyruvate formate-lyase activating enzyme. Proc. Natl. Acad. Sci. USA. 2008; 105:16137–16141. [PubMed: 18852451]
15. Holm L, Rosenström P. Dali server: conservation mapping in 3D. Nucleic Acids Res. 2010; 38:W545–W549. [PubMed: 20457744]
16. Farrar CE, Jarrett JT. Protein residues that control the reaction trajectory in *S*?adenosylmethionine radical enzymes: Mutagenesis of asparagine 153 and aspartate 155 in *Escherichia coli* biotin synthase. Biochemistry. 2009; 48:2448–2458. [PubMed: 19199517]
17. Harding MM. Small revisions to predicted distances around metal sites in proteins. ActaCrystallogr.D Biol. Crystallogr. 2006; 62:678–682.
18. Zheng H, Chruszcz M, Lasota P, Lebioda L, Minor W. Data mining of metal ion environments present in protein structures. J. Inorg. Biochem. 2008; 102:1765–1776. [PubMed: 18614239]
19. Walden H, et al. Tiny TIM: A small, tetrameric, hyperthermostable triosephosphate isomerase. J. Mol. Biol. 2001; 306:745–757. [PubMed: 11243785]
20. Nagano N, Orengo CA, Thornton JM. One fold with many functions: The evolutionary relationships between TIM barrel families based on their sequences, structures and functions. J. Mol. Biol. 2002; 321:741–765. [PubMed: 12206759]
21. Blair DE, van Aalten DMF. Structures of*Bacillus subtilis* PdaA, a family 4 carbohydrate esterase, and a complex with *N*-acetyl-glucosamine. FEBS Lett. 2004; 570:13–19. [PubMed: 15251431]
22. Romier C, Reuter K, Suck D, Ficner R. Crystal structure of tRNA-guanine transglycosylase: RNA modification by base exchange. EMBO J. 1996; 15:2850–2857. [PubMed: 8654383]
23. Huang K, Li Z, Jia Y, Dunaway-Mariano D, Herzberg O. Helix swapping between two α/β barrels: crystal structure of phosphoenolpyruvatemutase with bound Mg^{2+}-oxalate. Structure. 1999; 7:539–548. [PubMed: 10378273]
24. Takagi H, et al. Crystal structure of the ribonuclease P protein Ph1877p from hyperthermophilic archaeon *Pyrococcus horikoshii* OT3. Biochem.Biophys. Res. Commun. 2004; 319:787–794. [PubMed: 15184052]
25. Teplyakov A, et al. Crystal structure of the *Escherichia coli* YcdX protein reveals a trinuclear zinc active site. Proteins. 2003; 51:315–318. [PubMed: 12661000]
26. Goldman A, Ollis DL, Steitz TA. Crystal structure of muconatelactonizing enzyme at 3 Å resolution. J. Mol. Biol. 1987; 194:143–153. [PubMed: 3612800]
27. Neidhart DJ, et al. Mechanism of the reaction catalyzed by mandelateracemase. 2. Crystal structure of mandelateracemase at 2.5-Å resolution: Identification of the active site and possible catalytic residues. Biochemistry. 1991; 30:9264–9273. [PubMed: 1892834]
28. Gromiha MM, Pujadas G, Magyar C, Selvaraj S, Simon I. Locating the stabilizing residues in $(\alpha/\beta)_8$ barrel proteins based on hydrophobicity, long-range interactions, and sequence conservation. Proteins. 2004; 55:316–329. [PubMed: 15048825]
29. Chatterjee A, et al. Reconstitution of ThiC in thiamine pyrimidine biosynthesis expands the radical SAM superfamily. Nat. Chem. Biol. 2008; 4:758–765. [PubMed: 18953358]
30. McGlynn SE, et al. Identification and characterization of a novel member of the radical AdoMet enzyme superfamily and implications for the biosynthesis of the Hmdhydrogenase active site cofactor. J. Bacteriol. 2010; 192:595–598. [PubMed: 19897660]
31. Paraskevopoulou C, Fairhurst SA, Lowe DJ, Brick P, Onesti S. The Elongator subunit Elp3 contains a Fe_4S_4 cluster and binds S-adenosylmethionine. Mol. Microbiol. 2006; 59:795–806. [PubMed: 16420352]
32. Marsh EN, Melendez GDR. Adenosylcobalamin enzymes: Theory and experiment begin to converge. Biochim.Biophys.Acta. 2012; 1824:1154–1164. [PubMed: 22516318]
33. Toraya T, Honda S, Mori K. Coenzyme B_{12}-dependent dioldehydratase is a potassium ion-requiring calcium metalloenzyme: evidence that the substrate-coordinated metal ion is calcium. Biochemistry. 2010; 49:7210–7217. [PubMed: 20712378]
34. Shibata N, et al. Crystal structures of ethanolamine ammonia-lyasecomplexed with coenzyme B_{12} analogs and substrates. J. Biol. Chem. 2010; 285:26484–26493. [PubMed: 20519496]

35. Kamachi T, Doitomi K, Takahata M, Toraya T, Yoshizawa K. Catalytic roles of the metal ion in the substrate-binding site of coenzyme B_{12}-dependent dioldehydratase. Inorg.Chem. 2011; 50:2944–2952. [PubMed: 21388166]
36. Frey PA. Lysine 2,3-aminomutase: is adenosylmethionine a poor man′s adenosylcobalamin? FASEB J. 1993; 7:662–670. [PubMed: 8500691]
37. Goldman PJ, Grove TL, Booker SJ, Drennan CL. X-ray analysis of butirosin biosynthetic enzyme BtrN redefines structural motifs for AdoMet radical chemistry. Proc. Natl. Acad. Sci. USA. 2013; 110:15949–15954. [PubMed: 24048029]
38. Frazzon J, Fick JR, Dean DR. Biosynthesis of iron-sulphur clusters is a complex and highly conserved process. Biochem.Soc. Trans. 2002; 30:680–685. [PubMed: 12196163]
39. Otwinowski Z, Minor W. Processing of X-ray diffraction data in oscillation mode. Macromol. Crystallogr. A. 1997; 276:307–326.
40. Terwilliger TC, et al. Decision-making in structure solution using Bayesian estimates of map quality: the PHENIX AutoSol wizard. ActaCrystallogr.D Biol. Crystallogr. 2009; 65:582–601.
41. Vonrhein C, Blanc E, Roversi P, Bricogne G. Automated structure solution with autoSHARP. Methods Mol. Biol. 2007; 364:215–230. [PubMed: 17172768]
42. Emsley P, Cowtan K. *Coot*: model-building tools for molecular graphics. ActaCrystallogr.D Biol. Crystallogr. 2004; 60:2126–2132.
43. Schröder GF, Levitt M, Brunger AT. Super-resolution biomolecular crystallography with low-resolution data. Nature. 2010; 464:1218–1222. [PubMed: 20376006]
44. Brunger AT, et al. Crystallography & NMR system: A new software suite for macromolecular structure determination. ActaCrystallogr.D Biol. Crystallogr. 1998; 54:905–921.
45. Brunger AT. Version 1.2 of the Crystallography and NMR system. Nat. Protoc. 2007; 2:2728–2733. [PubMed: 18007608]
46. Adams PD, et al. PHENIX: a comprehensive Python-based system for macromolecular structure solution. ActaCrystallogr.D Biol. Crystallogr. 2010; 66:213–221.
47. French S, Wilson K. On the treatment of negative intensity observations .Acta Crystallogr. A. A34:517–525.
48. Winn MD, et al. Overview of the CCP4 suite and current developments. ActaCrystallogr.D Biol. Crystallogr. 2011; 67:235–242.
49. Painter J, Merritt EA. Optimal description of a protein structure in terms of multiple groups undergoing TLS motion. ActaCrystallogr.D Biol. Crystallogr. 2006; 62:439–450.
50. Painter J, Merritt EA. *TLSMD* web server for the generation of multi-group TLS models. J. Appl. Cryst. 2006; 39:109–111.
51. Laskowski RA, MacArthur MW, Moss DS, Thornton JM. PROCHECK: a program to check the stereochemical quality of protein structures. J. Appl. Cryst. 1993; 26:283–291.
52. Baker NA, Sept D, Joseph S, Holst MJ, McCammon JA. Electrostatics of nanosystems: Application to microtubules and the ribosome. Proc. Natl. Acad. Sci. U. S. A. 2001; 98:10037–10041. [PubMed: 11517324]
53. Bond CS. TopDraw: a sketchpad for protein structure topology cartoons. Bioinformatics. 2003; 19:311–312. [PubMed: 12538265]
54. Lopes CT, et al. Cytoscape Web: an interactive web-based network browser. Bioinformatics. 2010; 26:2347–2348. [PubMed: 20656902]

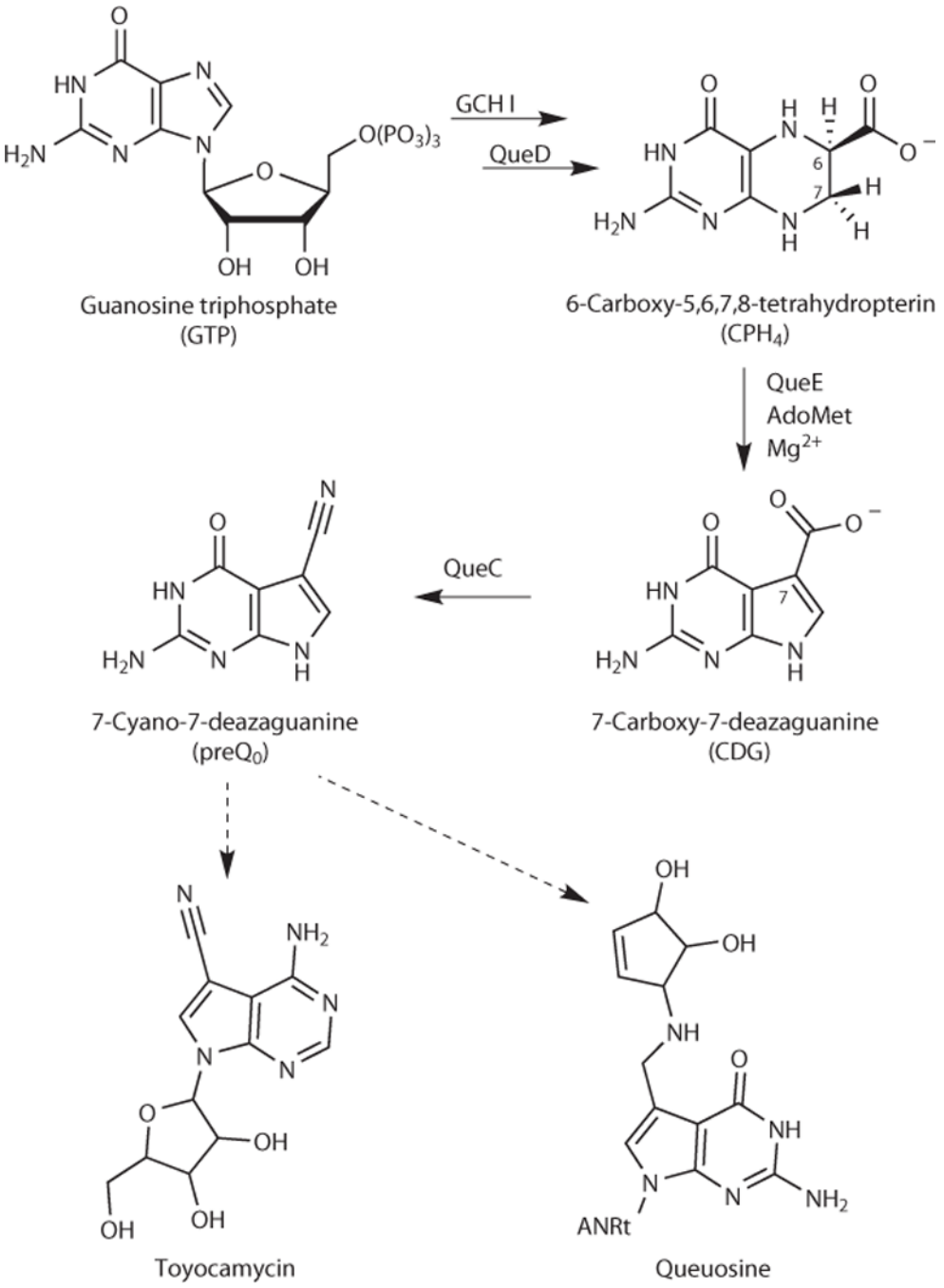

Figure 1. Biosynthetic pathway for the common precursor of all deazapurines, preQ$_0$

GTP is converted to CPH_4 by the sequential action of GCH I and QueD[6]. QueE catalyzes the AdoMet-and Mg^{2+}-dependent rearrangement of CPH_4 to CDG[10]. QueC catalyzes the ATP-dependent conversion of CDG and ammonia to preQ$_0$. Two deazapurine natural products derived from preQ$_0$ are depicted: the antibiotic toyocamycin and the ubiquitous hypermodified tRNA base queuosine.

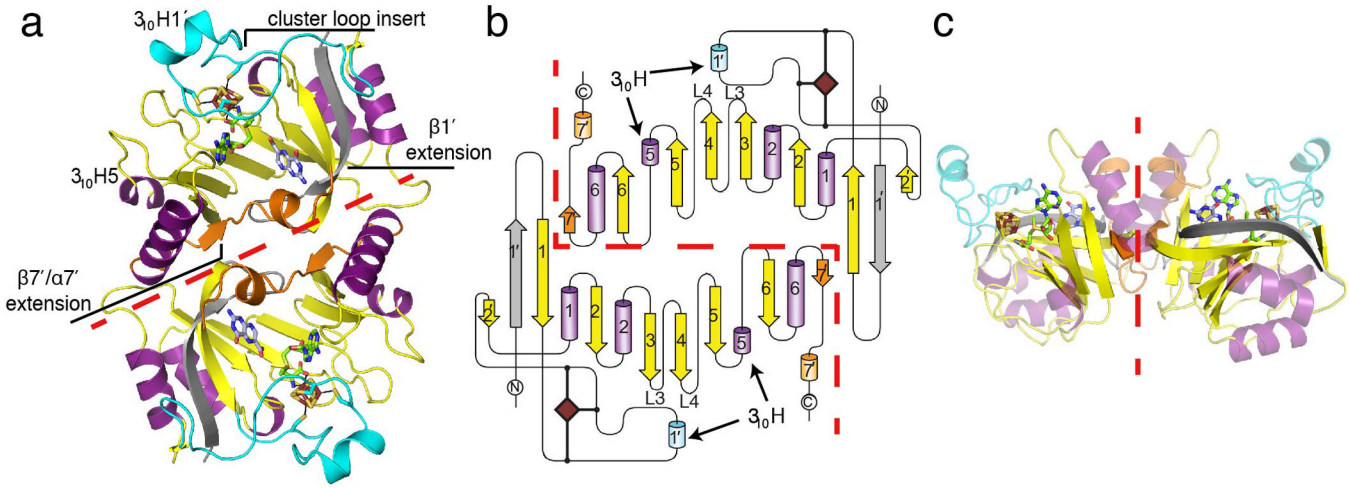

Figure 2. Overall structure of QueE

(**a**) Ribbon depiction of QueE dimer displayed with a red dashed line delineating the dimer interface, and cluster-binding loop with inserted 3_{10}-helix colored in cyan. The rest of the modified (β_6/α_3) core is colored in yellow for loops and strands and purple for helices, with N– and C–terminal extensions to the core colored gray and orange, respectively. Carbons for AdoMet and the 6CP ligand are colored green and light blue, respectively. Iron-sulfur cluster is in ruby and yellow sticks. Residues from the N– and C–terminal extensions primarily make up the dimer interface, in addition to α6. (**b**) Topology diagram of the QueE dimer is depicted, colored as in (a), with inter-monomeric 10-stranded β-sheets of 1′1234567′**11′** (bold and underline typesets indicate secondary structure from the dimer molecule and antiparallel β-strands, respectively, and the symbol prime denotes elements outside of the AdoMet radical protein core). 3_{10}-helices are assigned based on hydrogen bonding, and [4Fe-4S] clusters are indicated as brown diamonds. (**c**) Alternative view of QueE dimer, displayed as though looking along the red dotted line of (a).

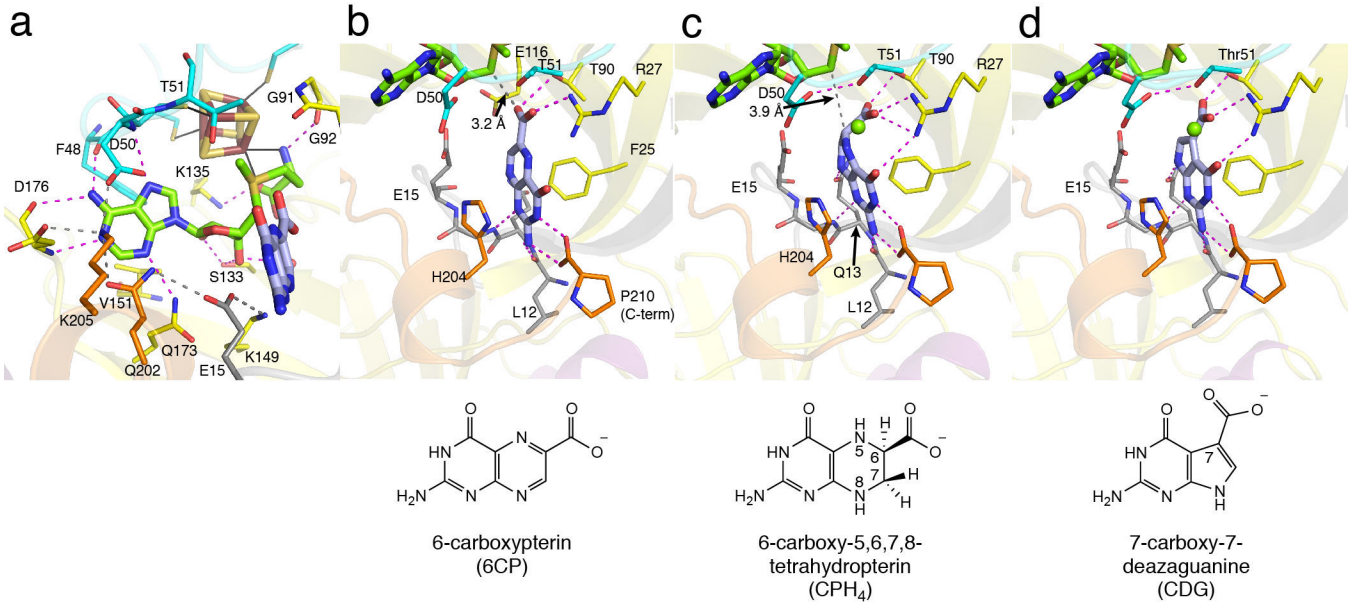

Figure 3. Binding of AdoMet, 6CP, CPH_4, and CDG

(**a**) The AdoMet binding pocket contains multiple hydrogen-bonding interactions, in addition to a protein hydrogen-bonding network located above the plane of the adenine (dashed gray lines)(see Supplementary Fig. 8 for stereoview). Coordination bonds to the iron-sulfur cluster are displayed as solid black lines. Protein-ligand interactions are represented as magenta dashed lines. Protein backbone is displayed as a transparent ribbon with ligand interacting residues as sticks. Protein carbons are colored cyan for the cluster-binding loop, yellow for the AdoMet radical core, gray for the N-terminal extension, and orange for the C-terminal extension. AdoMet and ligand carbons are colored green and light blue, respectively. (**b**) The substrate analogue 6CP is bound such that an oxygen of the C6-carboxylate moiety is positioned 3.2 Å from the C5′ of AdoMet (dashed gray line). (**c**) Binding of substrate, CPH_4, and Mg^{2+} ion (green sphere) in the 2.2 Å resolution structure positions C6 of the substrate 3.9 Å from the C5′ of AdoMet (dashed gray line). (**d**) Binding of product (CDG) and Mg^{2+} ion (green sphere) in the 1.9 Å resolution structure.

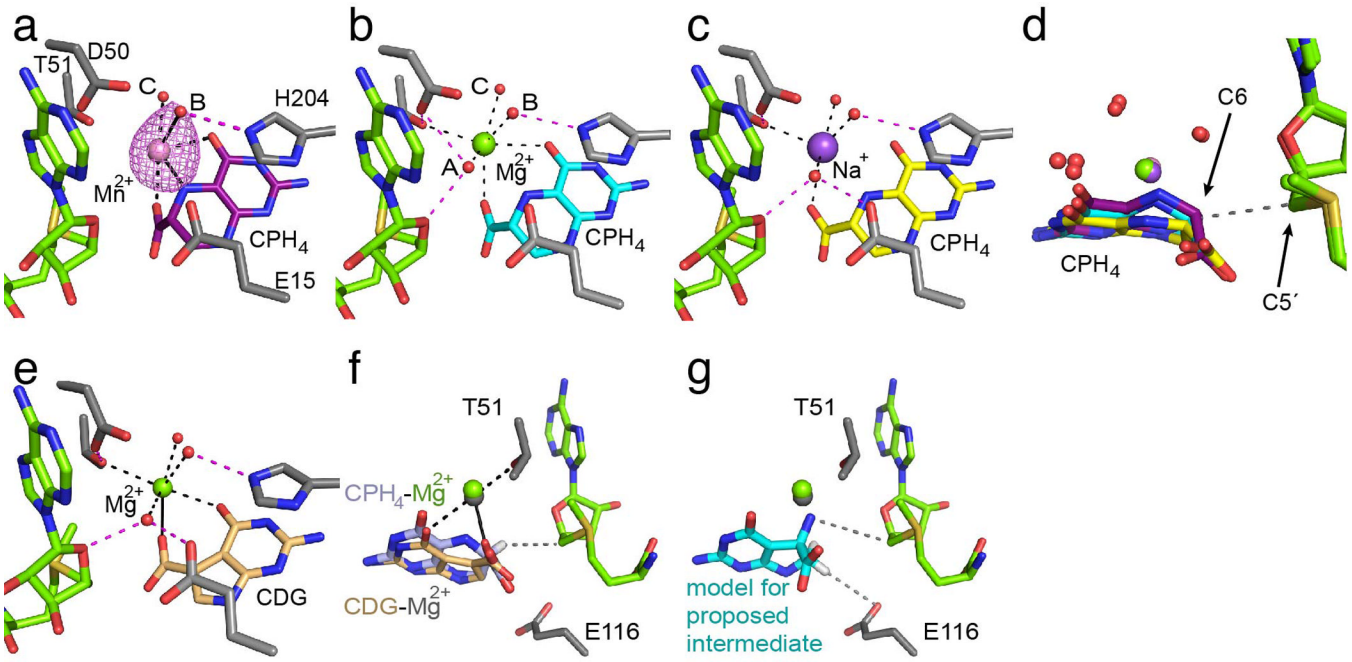

Figure 4. Metal ion interactions

(**a**–**c**) QueE structures with CPH_4 and different metals, colored as follows: (**a**) Mn^{2+}/CPH_4, pink/purple; (**b**) Mg^{2+}/CPH_4, green/cyan; and (**c**) Na^{+}/CPH_4, purple/yellow. Hydrogen bonding interactions with metal-bound water molecules are displayed as magenta dashed lines; coordination distances are shown as solid black lines; and metal-ligand distances between 2.5–3.2 Å are represented by dotted black lines. Distances are presented in Supplementary Table 4. Anomalous difference electron density for Mn^{2+} is contoured at 3σ (pink mesh). AdoMet carbons, green; protein carbons, gray; water, red spheres. (**d**) An overlay of all three CPH_4-bound structures, colored as in (a–c). The distance between C6 of the substrate and the C5′ of AdoMet is represented as a dashed gray line. (**e**) QueE cocrystallized with Mg^{2+}/CDG in green/tan; lines and other colors as in (a). (**f**) A superposition of substrate- and product-bound QueE colored as in (a) with Mg^{2+}/CPH_4 and Mg^{2+}/CDG in green/light blue and gray/tan, respectively. The distance (3.4 Å) between the AdoMet C5′ and the CPH_4 C6 H-atom is displayed as a dashed gray line. (**g**) The proposed exocyclic nitrogen-containing intermediate is modeled into the QueE active site with cyan carbons, based on the binding mode of CPH_4 to preserve reasonable distances to the metal ion-binding site. This orientation positions the proposed nitrogen radical within reasonable distance (~ 4 Å) to the C5′ of AdoMet, displayed as a dashed gray line, for re-abstraction of an H-atom to regenerate AdoMet cofactor. The distance (~ 3.5 Å) between the C7 proton to be lost in the reaction and the nearest protein residue, E116, is also represented as a dashed gray line.

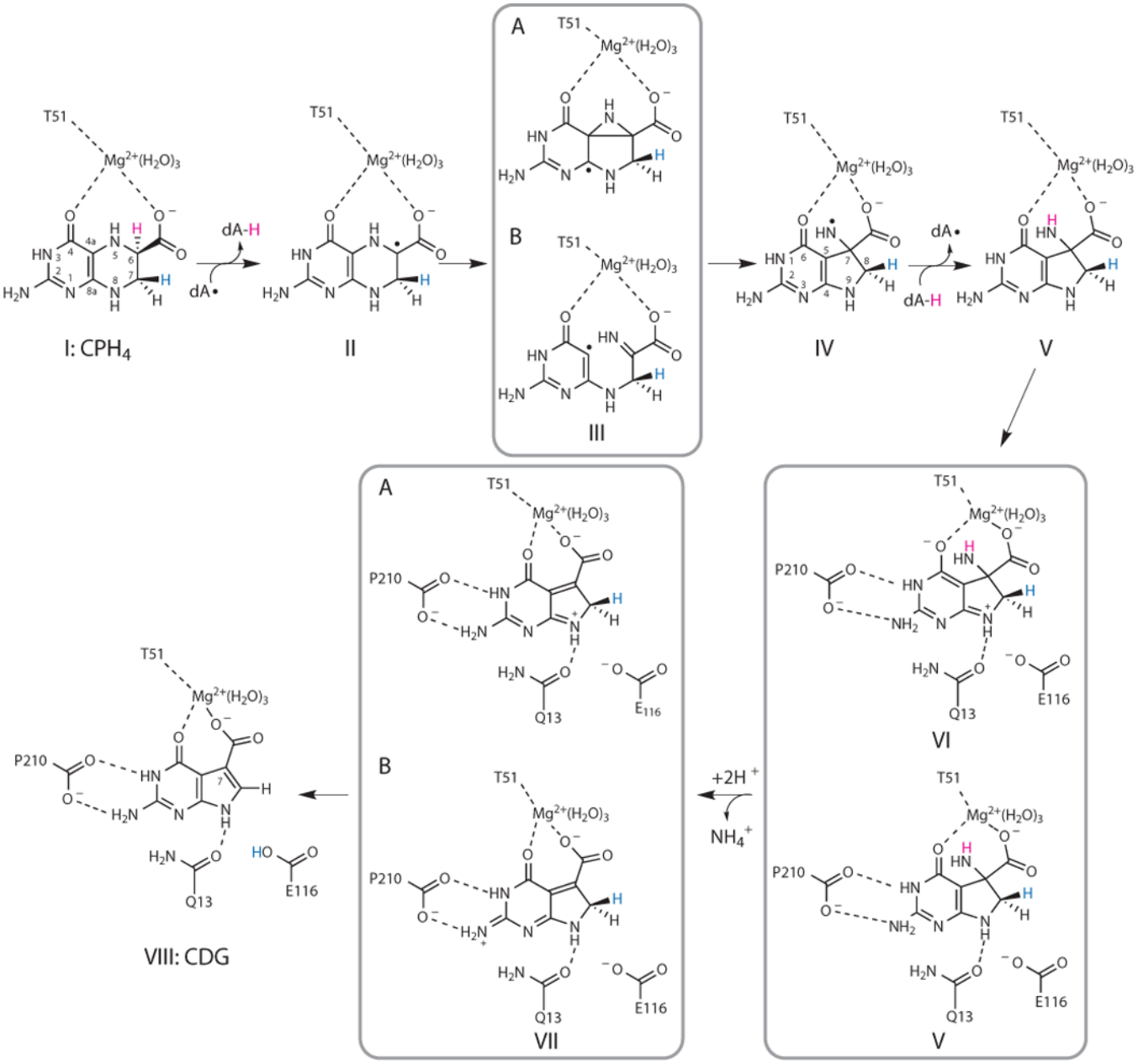

Figure 5. Proposed mechanism for QueE

The fates of hydrogen atoms colored in blue or magenta have been confirmed by isotope labeling studies[10]. Steps are described in the text.